Alexandria Engineering Journal 107 (2024) 559–567

Contents lists available at ScienceDirect

Alexandria Engineering Journal

journal homepage: www.elsevier.com/locate/aej

Original article

Performance optimization for hybrid TS/PS SWIPT UAV in cooperative NOMA IoT networks

Van Nhan Vo [a,b], Viet-Hung Dang [a,b], Hung Tran [c], Duc-Dung Tran [d], Symeon Chatzinotas [d], Hai Le Quoc [e], Chakchai So-In [f], Van-Truong Truong [g,b], Tu Dac Ho [h,i,*]

[a] Faculty of Information Technology, Duy Tan University, Da Nang 550000, Viet Nam
[b] Institute of Research and Development, Duy Tan University, Da Nang 550000, Viet Nam
[c] DATCOM Lab, Faculty of Data Science and Artificial Intelligence, College of Technology, National Economics University, Hanoi 12116, Viet Nam
[d] Interdisciplinary Center for Security, Reliability and Trust (SnT), University of Luxembourg, Esch-sur-Alzette 4365, Luxembourg
[e] Department of Information Technology, Quang Tri College, Quang Tri 520000, Viet Nam
[f] Applied Network Technology (ANT), College of Computing, Khon Kaen University, Khon Kaen 40002, Thailand
[g] Faculty of Electrical and Electronic Engineering, Duy Tan University, Da Nang 550000, Viet Nam
[h] Faculty of Information Technology and Electrical Engineering, NTNU- Norwegian University of Science and Technology, Trondheim 7491, Norway
[i] Faculty of Engineering Science and Technology, UiT- The Arctic University of Norway, Narvik 8514, Norway

ARTICLE INFO

Keywords:
Hybrid TS/PS
Cooperative NOMA
Outage probability
UAV
Bat algorithm optimization

ABSTRACT

This study examines a cooperative non-orthogonal multiple access (NOMA) network utilizing an energy-constrained unmanned aerial vehicle (UAV) relay (UAVR) to expand coverage and improve network throughput. In order to provide energy to the UAVR, we consider the hybrid simultaneous wireless information and power transmission (SWIPT) method, which allows the UAVR to harvest energy from the source (i.e., sink node) signal. Herein, a hybrid time switching (TS)-based and power splitting (PS)-based relaying scheme is applied to improve the UAVR's energy harvesting (EH) efficiency and the system performance. Given this context, we derive the closed-form expression of the outage probability (OP) for the sensors to evaluate the network performance. Based on the achieved analytical results, we apply the bat algorithm optimization (BAO) method to determine the optimal working point (as a fraction of received power and power allocation coefficients, and the 3-D positions of the UAVR) for the system such that the OP is minimized. The numerical analysis indicates that BAO is effective in both exploring and exploiting solutions, making it a suitable choice for similar non-convex optimization problems in continuous search spaces for cooperative NOMA IoT networks.

1. Introduction

Unmanned aerial vehicle (UAV)-assisted communications has recently emerged as a crucial aspect of Internet of Things (IoT) networks. This is primarily due to their ability to adjust their altitudes and navigate around obstacles, as highlighted by [1,2]. Moreover, UAVs offer an adaptable and cost-effective solution for extending the coverage and enhancing the throughput of existing terrestrial cellular networks. This is achieved by circumventing obstructions such as buildings, mountains, and forests, while also expanding the potential for providing line-of-sight (LoS) connectivity to end-users on the ground, as noted in [3,4].

Unfortunately, UAVs are battery-operated devices with a limited battery life, and their power consumption significantly impacts the communication process, as highlighted by various studies such as [5–7]. Therefore, the use of radio frequency (RF) EH techniques presents a reliable solution to address the power constraints faced by UAVs. For instance, in [8], the author proposed an RF EH UAV network enabling the UAV to provide services to ground customers while also gathering energy from charging stations through the wireless power transfer (WPT) technique.

In the WPT technique, there are two standard protocols: time-splitting-based relaying (TS) and power-splitting-based relaying (PS) [9–11]. In particular, the TS protocol includes a switcher at the receiver that regularly switches between the state of information decoding and EH. In the PS protocol, a power splitter at the receiver divides the received signal into two parts. One half is for EH, while the other is for information decoding. Recent research focuses on both because they are equally significant. Furthermore, there is no definitive answer as to

* Corresponding author at: Faculty of Information Technology and Electrical Engineering, NTNU- Norwegian University of Science and Technology, Trondheim 7491, Norway.
E-mail address: tu.d.ho@ntnu.no (T.D. Ho).

https://doi.org/10.1016/j.aej.2024.07.054
Received 22 December 2023; Received in revised form 11 April 2024; Accepted 14 July 2024
Available online 29 July 2024

which is preferable. For example, the TS protocol outperforms the PS protocol at low SNR, while the PS protocol outperforms the TS protocol at high SNR [9]. In contrast to standard PS and TS protocols, alternative TS and PS protocols that may have less implementation complexity, need less channel knowledge and increase the system performance are available in the literature [10,11]. However, these new protocols do not outperform the standard TS or PS protocols under all network conditions. Therefore, an enhanced protocol, known as hybrid EH, which combines TS and PS, where the received signal will be first switched for EH and then switched to the power splitter frequently. The author in [12] concluded that this protocol does not only improve the EH efficiency and the system performance but also outperforms both the TS and PS protocols. Obviously, the UAV, with the energy constraints, will have better performance when using the hybrid EH compared to using conventional EH methods.

On the one hand, non-orthogonal multiple access (NOMA) has been widely recognized as a promising solution to improve system performance and spectrum access efficiency in massive access scenarios [13–18]. For instance, [16] examined a multi-user communication system, in which a UAV base station utilizes NOMA to provide services to a vast number of ground users. Specifically, this work formulated a max–min rate optimization problem for many users and proposed a path-following algorithm to address it. As per the quantitative results, NOMA outperforms orthogonal multiple access (OMA) in terms of system performance. Additionally, [19] considered the use of a UAV as a relay (referred to as UAVR) to transmit information from its sources to its final destinations. The numerical results demonstrate that optimal OP can be achieved by strategically placing the UAVR and adjusting the transmission power of both the source and the UAVR.

On the other hand, some studies have explored the use of cooperative NOMA and EH because of its ability to increase spectral efficiency and system performance [18,20]. Building on this research, [20] proposed a hybrid EH protocol for cooperative NOMA to enhance the system performance of existing EH protocols with a more practical approach. The study investigated optimal power allocation factors for the hybrid protocol, and the results demonstrated the superiority of the proposed cooperative NOMA compared to other methods. However, previous research has assumed perfect channel state information (CSI) of the channels, which is unrealistic. Therefore, this paper examines the performance of EH UAVR cooperative NOMA networks with imperfect CSI of the channels.

Besides, we will use a minimization method to identify the suboptimal working point for the system parameters and the 3D position of the UAV Relay, based on the closed-form expression we derived for the OP. As the OP is non-convex and may have multiple local minima, gradient-based methods are unsuitable. Instead, heuristic search methods are employed, such as simulated annealing (SA), genetic algorithms (GA), or particle swarm optimization (PSO) [21–26]. These methods use a combination of downhill climbing search and local random search to escape local minima and achieve good minima results. However, SA only updates one individual over time, which limits its exploration ability.

Meanwhile, GA and PSO control a set of individuals (called a population) to collaborate with each other for the search and reach some better balance of exploration and exploitation [27,28]. However, GA usually works with two interchangeable domains, i.e., the chromosome domain and the search space domain. The chromosomal domain is usually discrete where the crossover and mutation steps are performed. Contrariwise, the search space domain is frequently continuous, with fitness evaluations performed for the selection step. Meanwhile, GA has to discretize the search space, and the precision is based on the resolution of this step. In addition, interpreting between search domain and chromosome domain is sometimes complicated. PSO works within just one continuous domain, in which the best individual is always stored to navigate the whole population. PSO, with its more greedy nature than GA, usually gives a quick convergence but a low-quality solution.

To address the aforementioned limitations, we will utilize the bat algorithm optimization (BAO) to determine the optimal working point for the system by minimizing the OP [29]. BAO is a population-based heuristic approach inspired by the natural echolocation-based hunting behavior of micro bat flocks. Each bat initially flies randomly and emits a pulse of a specific frequency, which reflects off objects or insects and is detected upon returning. Based on the echoes received, the bat modifies the pulse frequency and loudness to facilitate the search. The frequency increases and loudness decreases when the bat is close to the target food. In BAO, the bats cooperate by performing local random searches and moving towards the bat that has the highest potential of finding food. As a result, BAO eliminates the chromosome domain of GA and employs PSO's best individual navigation. Furthermore, BAO is less greedy than PSO as it enables more random search (exploration) by regulating the behavior of the entire population via the bats' pulse frequencies and pulse loudness.

Motivated by the above works, this work focuses on the optimization problem of system performance for the hybrid EH scheme, which combines TS and PS, in the context of cooperative NOMA IoT networks to improve the mentioned drawbacks. In this paper, we make the following primary contributions:

- We investigate a novel approach to optimizing the performance of UAV-assisted cooperative NOMA IoT networks using the hybrid SWIPT method that combines the TS and PS techniques. In our proposed system, a sink node transmits information to two sensor clusters having different priority levels. We also incorporate an EH UAVR to enhance system performance in scenarios where obstacles may be present.
- We propose a three-phase communication protocol for the cooperative NOMA IoT network with the hybrid TS/PS simultaneous wireless information and power transfer (SWIPT) scheme, consisting of the TS-based EH phase, the PS-based EH and direct information transmission phase, and the relaying transmission phase. Using this protocol, we derive a closed-form expression for the OP of the system.
- We propose employing the BAO method to determine the optimal values of the fraction of received power, power allocation coefficients, and the position of the UAVR. The objective is to minimize the OP of the system, as indicated by the analytical results obtained in terms of the OP.

The subsequent sections of this paper are structured in the following manner: Section 2 presents the system model and communication protocol. In Section 3, the closed-form expressions for the operational performance and the formulation of the optimization problem are presented. In Section 4, the authors introduce the BAO method as a proposed solution to the optimization problem. The findings obtained from the simulation are presented and analyzed in Section 5, while the conclusions drawn from the study are provided in Section 6.

2. System model and communication protocol

2.1. System model and channel assumptions

We consider the IoT architecture shown in Fig. 1 for downlink cooperative NOMA scenario. This can apply to such real-world scenarios as disasters and/or military sites where IoT devices (i.e., sensors) are hard to communicate directly with the sink and UAVR is used to maintain its information transmission. In particular, the sink uses the NOMA technique to transmit the signal to a UAVR and sensors, which are distributed into two clusters, i.e., a high-priority cluster and a low-priority cluster. In order to use energy efficiently, UAVR harvests energy and uses it to transfer the received information to the sensors.

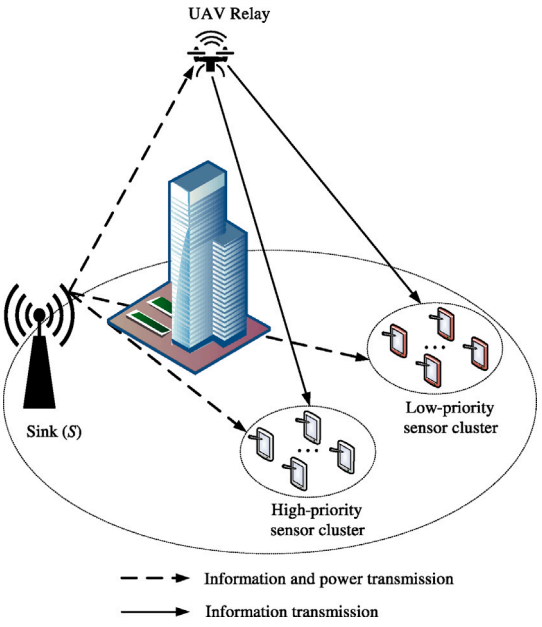

Fig. 1. Downlink cooperative NOMA.

It should be noted that both the sink and sensors are equipped with a solitary antenna, as this is necessitated by their respective sizes and limitations in terms of capability. In addition, the UAVR is outfitted with a multitude of antennas in order to enhance its EH capabilities. For sink-to-UAVR and UAVR-to-sensor communication, the models of path loss are presented in terms of absolute values as

$$\overline{L}_a = \beta_a d_a^{\eta_a}, \tag{1}$$

where $a \in \{SR_k, R_kU_i, R_kVj\}$ and $\eta_a = 2$. Depending on the environment, sink-to-UAVR and UAVR-to-sensor channels are more likely to be dominated by either LoS circumstances or non-line-of-sight (NLoS) situations (e.g., suburban, urban, or dense urban) [30]. Thus, the quantity β_a is formulated as $\beta_a = 10^B$ [31], in which B is defined as

$$B = \frac{10\log_{10}(4\pi f/c)^2 + \omega_{NLoS}}{10} + \frac{\omega_{LoS} - \omega_{NLoS}}{10 + 10\varphi\exp\left[-\psi\left(\frac{180}{\pi}\theta_a - \varphi\right)\right]}, \tag{2}$$

where θ_a is the UAVR elevation angle with respect to either the sink or sensors; φ and ψ are constants that depend on the environment [32]; and the extra path losses of LoS and NLoS connections are represented by the parameters ω_{LoS} and ω_{NLoS}, respectively, which depend on the surrounding environment and the transmission frequency [32]. Furthermore, the channel coefficients are assumed to be identically independent distributed (i.i.d) random variable (RV) following Nakagami-m distribution with fading severity parameter m. Therefore, the channel gains follow a Gamma distribution [7]. Given the uncertainty of the channel gains, appropriate probability density functions are established to represent this uncertainty. The Monte Carlo simulation is employed as a stochastic technique to model these uncertainties [33–36]. Thus, the probability density function (PDF) and cumulative distribution function (CDF) of the channel gain $|g_{XY}|^2$ are formulated as follows [37]:

$$f_{|g_{XY}|^2}(x) = \left(\frac{m_{XY}}{\Omega_{XY}}\right)^{m_{XY}} \frac{x^{m_{XY}-1}}{\Gamma(m_{XY})}\exp\left(-\frac{m_{XY}x}{\Omega_{XY}}\right), \tag{3}$$

$$F_{|g_{XY}|^2}(x) = 1 - \sum_{j=0}^{m_{XY}-1}\left(\frac{m_{XY}x}{\Omega_{XY}}\right)^j \frac{1}{j!}\exp\left(-\frac{m_{XY}x}{\Omega_{XY}}\right), \tag{4}$$

Table 1
Notations.

Notation	Definition
S	The sink
R_k	The kth antenna of UAVR, where $1 \le k \le K$
U_i	The ith high-priority sensor, where $1 \le i \le I$
V_j	The jth low-priority sensor, where $1 \le j \le J$
g_{XY}	The channel coefficient from X to Y, where $X, Y \in \{S, R_k, U_i, V_j\}$
$f_{\lvert g_{XY}\rvert^2}(\cdot)$	The PDF of the channel gain $\lvert g_{XY}\rvert^2$
$F_{\lvert g_{XY}\rvert^2}(\cdot)$	The CDF of the channel gain $\lvert g_{XY}\rvert^2$
$\Omega_{\lvert g_{XY}\rvert^2}$	The mean channel gain of the channel gain $\lvert g_{XY}\rvert^2$
d_{XY}	The distance from X to Y
$\overline{g}_{XY}$	The channel coefficient estimated using the minimum mean square error (MMSE) for g_{XY}

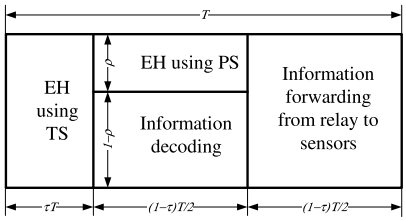

Fig. 2. Illustration of a hybrid TS/PS SWIPT-based decode-and-forward (DF) UAVR strategy.

where $X, Y \in \{S, R_k, U_i, V_j\}$, g_{XY} is an RV with the mean value of $\Omega_{XY} = \mathbf{E}\left[|g_{XY}|^2\right]$, and $\Gamma(\cdot)$ is the Gamma function. In addition, the imperfect CSI of the channel gains are considered as follows [38]:

$$g_{XY} = \overline{g}_{XY} + e_{XY}, \tag{5}$$

where $\overline{g}_{XY}$ represents the estimated channel coefficient and $e_{XY} \in \mathcal{CN}\left(0, \sigma_{XY}^2\right)$ denotes the channel estimation error; and $\hat{\Omega}_{XY} = \left(1 - \phi_{XY}\right)\Omega_{XY}$, $\phi_{XY} = \frac{\sigma_{XY}^2}{\Omega_{XY}}$ denotes the relative channel estimation error. The main notations used to describe the system model are listed in Table 1.

2.2. Communication protocol

This subsection presents the communication protocol for the downlink scenario. In order to improve the system performance, a hybrid TS/PS SWIPT is adopted at the UAVR cluster for the downlink scenario, as shown in Fig. 2. In particular, a block of time T is divided into three phases. During the first phase, denoted as τT, UAVR harvests energy from their sink, where $0 < \tau < 1$ denotes the fraction of block time for EH in the downlink scenario. During the second phase, denoted as $(1-\tau)T/2$, the chosen antenna of the UAVR employs a portion ρ of the received power for EH, while the remaining fraction $(1-\rho)$ is allocated for information decoding. Here, ρ represents the power-splitting ratio, which satisfies the condition $0 < \rho < 1$. During the third phase, denoted as $(1-\tau)T/2$, the UAVR employs the energy it has harvested to transmit the received signal to the sensors.

Based on this time frame, the downlink scenario of the considered system is deployed in three phases, namely the EH phase and direct information transmission phase (the first), information decoding phase (the second phase), and the relaying transmission phase (the third phase), as follows:

- In the first phase, i.e., EH and direct information transmission phase, the sink broadcasts the superposed signal, i.e., $\sqrt{\alpha_{U_i}}x_{U_i} + \sqrt{\alpha_{V_j}}x_{V_j}$, to sensors and UAVR by applying the principle of NOMA [39]. Herein, x_{U_i} and x_{V_j}, and α_{U_i} and α_{V_j} are the intended

transmit signals and power allocation coefficients of the sensors U_i and V_j at the sink, respectively, where $\alpha_{U_i} + \alpha_{V_j} = 1$ and $\alpha_{U_i} > \alpha_{V_j} > 0$. Furthermore, a sensor in each cluster is selected based on the channel quality of the direct link, in which the worst channel is chosen instead of the best one to guarantee that all sensors that can receive the information from the sink, i.e.,

$$i^* = \min_{1\le i\le I}\left\{\left|g_{SU_i}\right|^2\right\} = \min_{1\le i\le I}\left\{\left|\hat{g}_{SU_i}\right|^2\right\}, \tag{6}$$

$$j^* = \min_{1\le j\le J}\left\{\left|g_{SV_j}\right|^2\right\} = \min_{1\le j\le J}\left\{\left|\hat{g}_{SV_j}\right|^2\right\}. \tag{7}$$

Therefore, the received signal at sensor A can be expressed as

$$y_{SA} = \left(\sqrt{\frac{\alpha_{U_{i^*}} P_S}{d_{SA}^{\theta_{SA}}}} x_{U_{i^*}} + \sqrt{\frac{\alpha_{V_{j^*}} P_S}{d_{SA}^{\theta_{SA}}}} x_{V_{j^*}}\right) g_{SA} + n_{SA}, \tag{8}$$

where $A \in \{U_{i^*}, V_{j^*}\}$, $n_{SA} \sim \mathcal{CN}(0, N_0)$, and N_0 is additive white Gaussian noise [40]. Accordingly, the signal-to-interference-plus-noise ratios (SINRs) for decoding the received signal at U_{i^*} and V_{j^*} are

$$\gamma_{SU_{i^*}}^{x_{U_{i^*}}} = \frac{\alpha_{U_{i^*}}\gamma_0\left|\hat{g}_{SU_{i^*}}\right|^2}{\alpha_{V_{j^*}}\gamma_0\left|\hat{g}_{SU_{i^*}}\right|^2 + \gamma_0\sigma_{SU_{i^*}}^2 + 1}, \tag{9}$$

$$\gamma_{SV_{j^*}}^{x_{U_{i^*}}} = \frac{\alpha_{U_{i^*}}\gamma_0\left|\hat{g}_{SV_{j^*}}\right|^2}{\alpha_{V_{j^*}}\gamma_0\left|\hat{g}_{SV_{j^*}}\right|^2 + \gamma_0\sigma_{SV_{j^*}}^2 + 1}, \tag{10}$$

$$\gamma_{SV_{j^*}}^{x_{V_{j^*}}} = \frac{\alpha_{V_{j^*}}\gamma_0\left|\hat{g}_{SV_{j^*}}\right|^2}{\gamma_0\sigma_{SV_{j^*}}^2 + 1}, \tag{11}$$

where $\gamma_0 = \frac{P_S}{N_0}$ and $\left|\hat{g}_{SA}\right|^2 = \left|\overline{g}_{SA}\right|^2 / d_{SA}^{\theta_{SA}}$. Similar to (8), the received signal at the kth antenna of the UAVR R_k is formulated as

$$y_{SR_k} = \left(\sqrt{\frac{\alpha_{U_{i^*}} P_S}{\overline{L}_{SR_k}}} x_{U_{i^*}} + \sqrt{\frac{\alpha_{V_{j^*}} P_S}{\overline{L}_{SR_k}}} x_{V_{j^*}}\right) g_{SR_k} + n_{SR_k}, \tag{12}$$

where $n_{SR_k} \sim \mathcal{CN}(0, N_0)$. Thus, the EH at the kth antenna of the UAVR in the first phase is given by

$$E_{R_k}^{(1)} = \eta\tau T P_S\left|\hat{g}_{SR_k}\right|^2, \tag{13}$$

where $\left|\hat{g}_{SR_k}\right|^2 = \left|\overline{g}_{SR_k}\right|^2 / \overline{L}_{SR_k}$.

- In the second phase, for information decoding, the received signal at kth antenna of the UAVR becomes

$$y_{SR_k} = \sqrt{1-\rho}\left(\sqrt{\frac{\alpha_{U_{i^*}} P_S}{\overline{L}_{SR_k}}} x_{U_{i^*}} + \sqrt{\frac{\alpha_{V_{j^*}} P_S}{\overline{L}_{SR_k}}} x_{V_{j^*}}\right) \times g_{SR_k} + n_{SR_k}. \tag{14}$$

Therefore, the EH during the second phase can be written as

$$E_{R_k}^{(2)} = \rho\eta(1-\tau) T P_S\left|\hat{g}_{SR_k}\right|^2/2. \tag{15}$$

Furthermore, the SINRs for decoding $x_{U_{i^*}}$ and $x_{V_{j^*}}$ can be written, respectively, as follows:

$$\gamma_{SR_k}^{x_{U_{i^*}}} = \frac{(1-\rho)\,\alpha_{U_{i^*}}\gamma_0\left|\hat{g}_{SR_k}\right|^2}{(1-\rho)\,\alpha_{V_{j^*}}\gamma_0\left|\hat{g}_{SR_k}\right|^2 + (1-\rho)\,\gamma_0\sigma_{SR_k}^2 + 1}, \tag{16}$$

$$\gamma_{SR_k}^{x_{V_{j^*}}} = \frac{(1-\rho)\,\alpha_{V_{j^*}}\gamma_0\left|h_{SR_k}\right|^2}{(1-\rho)\,\gamma_0\sigma_{SR_k}^2 + 1}. \tag{17}$$

- In the third phase, i.e., the relaying transmission phase, the energy harvested is utilized as transmit power for the relaying transmission. Specifically, using the hybrid TS/PS SWIPT method, the total amount of energy collected at the kth antenna of the UAVR can be shown mathematically as follows: [20]

$$E_{R_k} = E_{R_k}^{(1)} + E_{R_k}^{(2)}. \tag{18}$$

Thus, the received signal at the Ath sensor in the second phase can be written as

$$y_{R_kA} = \left(\sqrt{\frac{\beta_{U_{i^*}} P_{R_k}}{\bar{L}_{R_kA}}} x_{U_{i^*}} + \sqrt{\frac{\beta_{V_{j^*}} P_{R_k}}{\bar{L}_{R_kA}}} x_{V_{j^*}}\right) g_{R_kA} + n_{R_kA}, \tag{19}$$

where $n_{R_kA} \sim \mathcal{CN}(0, N_0)$; $\beta_{U_i^*}$ and $\beta_{V_j^*}$ are the power allocation coefficients of the sensors U_i and V_j at the UAVR, respectively and $\beta_{U_i^*} + \beta_{V_j^*} = 1$ and $\beta_{U_i^*} > \beta_{V_j^*} > 0$; and the transmit power of UAVR at the kth antenna R_k in the transmission phase with the hybrid TS/PS SWIPT is [20]

$$P_{R_k} = \frac{E_{R_k}}{(1-\tau)T/2} = \eta P_S\left|\hat{g}_{SR_k}\right|^2\left(\frac{2\tau}{1-\tau} + \rho\right). \tag{20}$$

Here, the fixed-gain EH is applied [41], i.e.,

$$P_{R_k} = \eta P_S \mathbb{E}\left\{\left|\hat{g}_{SR_k}\right|^2\right\}\left(\frac{2\tau}{1-\tau} + \rho\right), \tag{21}$$

where $\mathbb{E}\left\{\left|\hat{g}_{SR_k}\right|^2\right\} = \lambda_{SR_k}$, which is defined as

$$\lambda_{SR_k} = \frac{\hat{\Omega}_{SR_k}}{\overline{L}_{SR_k}} = \frac{\left(1-\phi_{SR_k}\right)\Omega_{SR_k}}{\overline{L}_{SR_k}}. \tag{22}$$

Therefore, the SINRs of U_{i^*} and V_{j^*} for decoding $x_{U_{i^*}}$ and $x_{V_{j^*}}$ are expressed as follows:

$$\gamma_{R_kU_{i^*}}^{x_{U_{i^*}}} = \frac{\beta_{U_{i^*}}\gamma_{R_k}\left|\hat{g}_{R_kU_{i^*}}\right|^2}{\beta_{V_{j^*}}\gamma_{R_k}\left|\hat{g}_{R_kU_{i^*}}\right|^2 + \gamma_{R_k}\sigma_{R_kU_{i^*}}^2 + 1}, \tag{23}$$

$$\gamma_{R_kV_{j^*}}^{x_{U_{i^*}}} = \frac{\beta_{U_{i^*}}\gamma_{R_k}\left|\hat{g}_{R_kV_{j^*}}\right|^2}{\beta_{V_{j^*}}\gamma_{R_k}\left|\hat{g}_{R_kV_{j^*}}\right|^2 + \gamma_{R_k}\sigma_{R_kV_{j^*}}^2 + 1}, \tag{24}$$

$$\gamma_{R_kV_{j^*}}^{x_{V_{j^*}}} = \frac{\beta_{V_{j^*}}\gamma_{R_k}\left|\hat{g}_{R_kV_{j^*}}\right|^2}{\gamma_{R_k}\sigma_{R_kV_{j^*}}^2 + 1}, \tag{25}$$

where $\left|\hat{g}_{R_kA}\right|^2 = \left|\overline{g}_{R_kA}\right|^2 / \overline{L}_{SR_k}$ and $\gamma_{R_k} = \frac{P_{R_k}}{N_0}$. Furthermore, the end-to-end SINR of the considered system can be given by

$$\gamma_{e2e}^{SR_kUV} = \min\left\{\gamma_{SR_k}^{x_{U_{i^*}}}, \gamma_{SR_k}^{x_{V_{j^*}}}, \gamma_{R_kU_{i^*}}^{x_{U_{i^*}}}, \gamma_{R_kV_{j^*}}^{x_{U_{i^*}}}, \gamma_{R_kV_{j^*}}^{x_{V_{j^*}}}\right\}. \tag{26}$$

In order to improve the OP, the selected kth antenna of the UAVR is chosen such that the end-to-end SINR is maximum, i.e.,

$$\gamma_{e2e}^{(d)} = \max_{1\le k\le K}\left\{\gamma_{e2e}^{SR_kUV}\right\}. \tag{27}$$

3. Performance analysis and optimization problem

The interruption of communication transmission can occur when both the direct SINR and the end-to-end SINR at the sensors fall below a predetermined outage threshold. Therefore, the OP of the considered system for the downlink scenario is defined as follows:

$$\begin{aligned}\mathcal{P} &= \mathcal{P}^U + \mathcal{P}^V - \mathcal{P}^{UV} \\ &= \mathcal{P}^{SRUV}\left(\mathcal{P}^{SU} - \mathcal{P}^{SU}\mathcal{P}^{SV} + \mathcal{P}^{SV}\right),\end{aligned} \tag{28}$$

where $\mathcal{P}^{SU}$, $\mathcal{P}^{SV}$, and $\mathcal{P}^{SU}$ are defined as

$$\mathcal{P}^{SU} = \Pr\left\{\gamma_{SU_{i*}}^{x_{U_{i*}}} < \varepsilon^{(d)}\right\}, \tag{29}$$

$$\mathcal{P}^{SV} = \Pr\left\{\gamma_{SV_{j*}}^{x_{U_{i*}}} < \varepsilon^{(d)}, \gamma_{SV_{j*}}^{x_{V_{j*}}} < \varepsilon^{(d)}\right\}, \tag{30}$$

$$\mathcal{P}^{SRUV} = \Pr\left\{\gamma_{e2e}^{(d)} < \varepsilon^{(d)}\right\}, \tag{31}$$

where $\varepsilon^{(d)} = 2^{2R} - 1$. Next, we will derive the probability $\mathcal{P}$. First, by substituting (9) into (29), we have

$$\mathcal{P}^{SU} = \Pr\left\{\frac{\alpha_{U_{i*}}\gamma_0\left|\hat{g}_{SU_{i*}}\right|^2}{\alpha_{V_{j*}}\gamma_0\left|\hat{g}_{SU_{i*}}\right|^2 + \gamma_0\sigma_{SU_{i*}}^2 + 1} < \varepsilon^{(d)}\right\}. \tag{32}$$

By utilizing the principles of probability and employing algebraic manipulations, Eq. (32) can be reformulated as

$$\mathcal{P}^{SU} = F_{\left|\hat{g}_{SU_{i*}}\right|^2}\left[\frac{\kappa_1\varepsilon^{(d)}}{\gamma_0\left(\alpha_{U_{i*}} - \alpha_{V_{j*}}\varepsilon^{(d)}\right)}\right], \tag{33}$$

where $\varepsilon^{(d)} < \frac{\alpha_{U_{i*}}}{\alpha_{V_{j*}}}$ and $\kappa_1 = \gamma_0\sigma_{SU_{i*}}^2 + 1$. By substituting the CDF of the channel gain $\left|\hat{g}_{SU_{i*}}\right|^2$ into (33), we obtain

$$\mathcal{P}^{SU} = 1 - \sum_{p=0}^{m_{SU_{i*}}-1}\frac{m_{SU_{i*}}^p}{p!\lambda_{SU_{i*}}^p}e^{-\frac{m_{SU_{i*}}\kappa_1\varepsilon^{(d)}}{\lambda_{SU_{i*}}\gamma_0\left(\alpha_{U_{i*}} - \alpha_{V_{j*}}\varepsilon^{(d)}\right)}} \times\left[\frac{\kappa_1\varepsilon^{(d)}}{\gamma_0\left(\alpha_{U_{i*}} - \alpha_{V_{j*}}\varepsilon^{(d)}\right)}\right]^p, \tag{34}$$

where $\lambda_{SU_{i*}}$ is defined as

$$\lambda_{SU_{i*}} = \frac{\hat{\Omega}_{SU_{i*}}}{d_{SU_{i*}}^{\theta_{SU_{i*}}}} = \frac{\left(1 - \phi_{SU_{i*}}\right)\Omega_{SU_{i*}}}{d_{SU_{i*}}^{\theta_{SU_{i*}}}}. \tag{35}$$

Similarly, by substituting (10) and (11) into (30) and using some algebraic manipulations, we have

$$\mathcal{P}^{SV} = 1 - \Pr\left\{\frac{\alpha_{U_{i*}}\gamma_0\left|\hat{g}_{SV_{j*}}\right|^2}{\alpha_{V_{j*}}\gamma_0\left|\hat{g}_{SV_{j*}}\right|^2 + \gamma_0\sigma_{SV_{j*}}^2 + 1} \geq \varepsilon^{(d)}, \frac{\alpha_{V_{j*}}\gamma_0\left|\hat{g}_{SV_{j*}}\right|^2}{\gamma_0\sigma_{SV_{j*}}^2 + 1} \geq \varepsilon^{(d)}\right\} = F_{\left|\hat{g}_{SV_{j*}}\right|^2}\left(\frac{\kappa_2\varepsilon^{(d)}}{\gamma_0\chi_1}\right), \tag{36}$$

where $\chi_1 = \min\left\{\alpha_{V_{j*}}, \alpha_{U_{i*}} - \alpha_{V_{j*}}\varepsilon^{(d)}\right\}$ and $\kappa_2 = \gamma_0\sigma_{SV_{j*}}^2 + 1$. Thus, the probability $\mathcal{P}^{SV}$ is obtained as

$$\mathcal{P}^{SV} = 1 - \sum_{p=0}^{m_{SV_{j*}}-1}\frac{m_{SV_{j*}}^p}{p!\lambda_{SV_{j*}}^p}\left(\frac{\kappa_2\varepsilon^{(d)}}{\gamma_0\chi_1}\right)^p e^{-\frac{m_{SV_{j*}}\kappa_2\varepsilon^{(d)}}{\lambda_{SV_{j*}}\gamma_0\chi_1}}, \tag{37}$$

where $\lambda_{SV_{j*}}$ is defined as

$$\lambda_{SV_{j*}} = \frac{\hat{\Omega}_{SV_{j*}}}{d_{SV_{j*}}^{\theta_{SV_{j*}}}} = \frac{\left(1 - \phi_{SV_{j*}}\right)\Omega_{SV_{j*}}}{d_{SV_{j*}}^{\theta_{SV_{j*}}}}. \tag{38}$$

Next, substitute (26) and (27) into (31), we have

$$\mathcal{P}^{SRUV} = \Pr\left\{\max_{1\leq k\leq K}\left\{\min\left\{\gamma_{SR_k}^{x_{U_{i*}}}, \gamma_{SR_k}^{x_{V_{j*}}}, \gamma_{R_kU_{i*}}^{x_{U_{i*}}}, \gamma_{R_kV_{j*}}^{x_{U_{i*}}}, \gamma_{R_kV_{j*}}^{x_{V_{j*}}}\right\}\right\} < \varepsilon^{(d)}\right\} = \prod_{k=1}^{K}\left(1 - \Pr\left\{\gamma_{SR_k}^{x_{U_{i*}}} \geq \varepsilon^{(d)}, \gamma_{SR_k}^{x_{V_{j*}}} \geq \varepsilon^{(d)}, \gamma_{R_kU_{i*}}^{x_{U_{i*}}} \geq \varepsilon^{(d)}, \gamma_{R_kV_{j*}}^{x_{U_{i*}}} \geq \varepsilon^{(d)}, \gamma_{R_kV_{j*}}^{x_{V_{j*}}} \geq \varepsilon^{(d)}\right\}\right). \tag{39}$$

After some basic manipulations and applying the properties of probabilities, the probability $\mathcal{P}^{SRUV}$ is rewritten as

$$\mathcal{P}^{SRUV} = \prod_{k=1}^{K}(1 - \Xi), \tag{40}$$

where $a = 1-\rho$, $\kappa_4 = a\gamma_0\sigma_{SR_k}^2 + 1$, $\lambda_{SR_k} \geq \frac{\kappa_4\varepsilon}{a\gamma_0\chi_1}$, $\chi_1 = \min\left\{\alpha_{V_{j*}}\alpha_{U_{i*}} - \alpha_{V_{j*}}\varepsilon^{(d)}\right\}$, $\chi_2 = \beta_{U_{i*}} - \beta_{V_{j*}}\varepsilon^{(d)}$, $\chi_3 = \min\left\{\beta_{V_{j*}}, \chi_2\right\}$, and Ξ is defined as

$$\Xi = \left[1 - F_{\left|\hat{g}_{R_kU_{i*}}\right|^2}\left(\frac{\gamma_{R_k}\sigma_{R_kU_{i*}}^2\varepsilon^{(d)} + \varepsilon^{(d)}}{\left(\beta_{U_{i*}} - \beta_{V_{j*}}\varepsilon^{(d)}\right)\gamma_{R_k}}\right)\right] \times\left[1 - F_{\left|\hat{g}_{R_kV_{j*}}\right|^2}\left(\frac{\varepsilon^{(d)}\gamma_{R_k}\sigma_{R_kV_{j*}}^2 + \varepsilon^{(d)}}{\chi_3\gamma_{R_k}}\right)\right]. \tag{41}$$

Using the CDF of the channel $\left|\hat{g}_{R_kU_{i*}}\right|^2$ and $\left|\hat{g}_{R_kV_{j*}}\right|^2$, the closed-form expression for the probability Ξ is derived as

$$\Xi = 1 - \sum_{p=0}^{m_{R_kU_{i*}}-1}\sum_{q=0}^{m_{R_kV_{j*}}-1}\frac{m_{R_kU_{i*}}^p}{p!\lambda_{R_kU_{i*}}^p}\left[\frac{\gamma_{R_k}\sigma_{R_kU_{i*}}^2\varepsilon^{(d)} + \varepsilon^{(d)}}{\left(\beta_{U_{i*}} - \beta_{V_{j*}}\varepsilon^{(d)}\right)\gamma_{R_k}}\right]^p \times e^{-\frac{m_{R_kU_{i*}}\left(\gamma_{R_k}\sigma_{R_kU_{i*}}^2\varepsilon^{(d)} + \varepsilon^{(d)}\right)}{\lambda_{R_kU_{i*}}\left(\beta_{U_{i*}} - \beta_{V_{j*}}\varepsilon^{(d)}\right)\gamma_{R_k}}}\frac{m_{R_kV_{j*}}^q}{p!\lambda_{R_kV_{j*}}^p} \times\left(\frac{\varepsilon^{(d)}\gamma_{R_k}\sigma_{R_kV_{j*}}^2 + \varepsilon^{(d)}}{\chi_3\gamma_{R_k}}\right)^q e^{-\frac{m_{R_kV_{j*}}\left(\varepsilon^{(d)}\gamma_{R_k}\sigma_{R_kV_{j*}}^2 + \varepsilon^{(d)}\right)}{\lambda_{R_kV_{j*}}\chi_3\gamma_{R_k}}}, \tag{42}$$

where $\lambda_{R_kU_{i*}}$ and $\lambda_{R_kV_{j*}}$ are defined as

$$\lambda_{R_kU_{i*}} = \frac{\hat{\Omega}_{R_kU_{i*}}}{\overline{L}_{R_kU_{i*}}} = \frac{\left(1 - \phi_{R_kU_{i*}}\right)\Omega_{R_kU_{i*}}}{\overline{L}_{R_kU_{i*}}}, \tag{43}$$

$$\lambda_{R_kV_{j*}} = \frac{\hat{\Omega}_{R_kV_{j*}}}{\overline{L}_{R_kV_{j*}}} = \frac{\left(1 - \phi_{R_kV_{j*}}\right)\Omega_{R_kV_{j*}}}{\overline{L}_{R_kV_{j*}}}. \tag{44}$$

Finally, the crux of the optimization problem lies in determining not only the UAVR locations but also the power allocation and fraction of received power at the UAVR so as to ensure that the OP of the sensors is minimized. In particular, we optimize the fraction of received power and power allocation factors at the UAVR, i.e., ρ, α_{U_i}, β_{V_j}, and the 3-D positions of the UAVR. Thus, the optimization problem can be formulated in the following manner:

$$\min_{\lambda_i}\{\mathcal{P}\}, \tag{45}$$

$$\text{s.t. } 0 \leq \rho \leq 1, \tag{46}$$

$$\alpha_{U_i} + \alpha_{V_j} = 1, \tag{47}$$

$$\beta_{U_i} + \beta_{V_j} = 1, \tag{48}$$

where λ_i is a set of optimized parameters

$$\lambda_i = [\rho, \alpha_u, \beta_u, x, y, z]^T. \tag{49}$$

4. Bat algorithm optimization for the cooperative NOMA IoT network

To address the problem (45), we apply the BAO algorithm which has many advantages. Specifically, BAO is a population-based search and thus achieves faster convergence than individual search SA. Its recent variations do not require chromosome-solution interpretation. Besides, it is not as greedy as other heuristic population-based methods, or it allows more exploration and gives a higher probability of reaching a global solution.

Generally, similarly to other heuristic population-based methods, BAO controls the collaboration among the candidates in the population in order to address two requirements, including exploitation, i.e., making candidates better over generations, and exploration, i.e., allowing candidates to not move towards good candidates. Specifically, each

candidate, λ_i is considered a micro bat hunting for food. It emits a pulse at the rate f_i with the loudness A_i. If a bat is near the food, it increases the pulse rate and decreases the loudness. A bat far from the food would move towards the best candidate, i.e., the bat nearest to the food. The moving pace is dependent on the average loudness of the whole population.

Algorithm 1 describes the pseudo-code of the Bat Algorithm for our minimization problem. Specifically, BA initializes the maximum number of generations G for the search. It also randomly produces the whole population of N_λ of bats, i.e., solution candidates denoted with $\lambda_i^{(0)}$, and their respective velocities v_i, pulse frequencies f_i, pulse rates r_i, and loudnesses A_i. Based on the objective function $F(\lambda)$, all the bats are evaluated, and the best candidate λ_{best} is picked and stored.

For each generation, a bat randomly chooses a pace length to move towards the best bat via its random f_i as follows:

$$f_i = f_{min} + \beta(f_{max} - f_{min}), \tag{50}$$

$$v_i^{(t+1)} = v_i^{(t)} + f_i(\lambda_{best}^{(t)} - \lambda_i^{(t)}), \tag{51}$$

$$\lambda_i^{(t+1)} = \lambda_i^{(t)} + v_i^{(t+1)}, \tag{52}$$

where β is a uniformly random value in $[0, 1]$ and $v_i^{(t+1)}$ represents the velocity of the bat $\lambda_i^{(t)}$, which is composed of the inertia of the old $v_i^{(t)}$ and the steer towards the best candidate at the portion of $f_i(\lambda_{best}^{(t)} - \lambda_i^{(t)})$. These two Eqs. (51) and (52) basically allow greedy behaviors of the bats. Then, each bat creates its potential updated version $\lambda_j^{(t)*}$, at the probability of $(1 - r_i^{(t)})$ (see lines 7–11 of Algorithm 1), that is around some chosen good candidate.

$$\lambda_i^{(t)*} = \lambda_i^{(t)} + \epsilon \frac{1}{N_\lambda} \sum_{j=1}^{N_\lambda} A_j^{(t)}, \tag{53}$$

where ϵ is a random value within $[-1, 1]$, N_λ is the bat population size and $\frac{1}{N_\lambda} \sum_{i=1}^{N_\lambda} A_i^{(t)}$ is actually the mean loudness of the whole population at the tth generation. However, this potential updated version $\lambda_i^{(t)*}$ is accepted only if it is better than the current version $\lambda_i^{(t)}$ and a uniform value $rand()$ is less than the bat's loudness. If this happen, BA increases the pulse rate $r_i^{(t)}$ and decreases the loudness $A_i^{(t)}$.

$$r_i^{(t+1)} = r_i^{(0)}(1 - e^{-\gamma(t+1)}), \tag{54}$$

$$A_i^{(t+1)} = \alpha A_i^{(t)}. \tag{55}$$

In fact, the mechanism of using potential updated version of bats is actually a local search with random walks. Besides, $\lambda_i^{(t)*}$ is obviously accepted with lower and lower probability over generations. In other words, BA allows high probability of exploration at the beginning of the search and gradually focuses on exploitation later on. This guarantees the convergence while permitting random local search in order to escape from local minima.

Note that in real-world cooperative NOMA IoT networks, BAO optimization should be performed in the centralized mode at the sink because: (i) optimization must take a short time in order to guarantee the real-time adaptation to any changes; (ii) BAO is a population-based searching method that requires high computing power; and (iii) the sink has enough information about the whole network parameters to evaluate the objective function.

5. Numerical results

This section presents the numerical results used to analyze the OP and we then provide the optimization results for this OP of the cooperative NOMA IoT network. In particular, we consider the impact of the altitude of UAVR (h_R), the EH time (τ), the correctness of the channel estimation (Ω_e), the number of the low-priority sensor cluster (I), the number of the high-priority sensor cluster (J), and the number of UAVR antennas (K) on the OP at the Ath sensor.

Algorithm 1 BAO-based OP optimization

Initialization:
Generation limit G, t^{th}-generation $t = 0$
Bat population of $\lambda_i^{(0)}$, and their respective velocities $v_i^{(0)}$, pulse frequencies f_i, pulse rates $r_i^{(0)}$, and loudnesses $A_i^{(0)}$
Objective function to minimize $F(\lambda) = \mathcal{P}(\lambda)$ (see (45))
A randomly chosen bat to be the current best bat λ_{best}
repeat
for each bat i **do**
Adjust the frequency spectrum f_i (see (50)),
Update the bat velocities $v_i^{(t)}$, (see (51))
Update the bat position $\lambda_i^{(t)}$ (see (52))
if $rand() > r_i^{(t)}$ **then**
Choose a solution amongst the best solutions.
Generate new potential solution $\lambda_i^{(t)*}$ around the chosen best solution (see (53))
end if
if $rand() < A_i^{(t)}$ and $F(\lambda_i^{(t)}) < F(\lambda_{best}^{(t)})$ **then**
Replace $\lambda_i^{(t)}$ with $\lambda_i^{(t)*}$
Increase pulse rates $r_i^{(t)}$ (see(54))
Decrease loudnesses $A_i^{(t)}$ (see (49))
end if
end for
Rank the bats and update the current λ_{best}
$t = t + 1$
until $t > G$ **return** λ_{best} and $F(\lambda_{best})$

Table 2
Environments.

Parameters	Sub-urban	Urban	Dense-urban
φ	4.8860	9.6177	12.0870
ψ	0.4290	0.1581	0.1139
θ_{LoS}	0.1	1	1.6
θ_{NLoS}	21	20	23

We investigate the considered cooperative NOMA IoT system with the following system parameters, used for both analysis and simulation [31,40,42]: the carrier frequency to $f_c = 2$ GHz, the EH efficiency coefficient to $\delta = 0.8$, and the fading parameters to $m_{SR} = m_{RA} = m_{SA} = 2$. The EH time fraction is chosen as $\tau \in [0.1, 0.9]$; $\sigma_{XY}^2 = \sigma_e^2 \in \{0.01, 0.02, 0.03\}$, $\gamma_0 \in [-10, 10]$ (dB), and $h_R \in [0, 20]$. The system bandwidth is $W = 100$ MHz. The coordinates of the sink, UAVR, U_i, and V_j are $S(0, 0, 0)$, $UR(1, 1, h_R)$, $U_i(2, 3, 0)$, and $V_j(4, 5, 0)$, respectively. The outage threshold is $R = 0.1$ b/s. Moreover, we explore the scenario where the IoT architecture is used in sub-urban, urban, and dense-urban setting with the parameters as Table 2 [43].

From Figs. 3 to 6 show the results of two methods: the solid lines are the probability calculated by using closed form, and the discrete points are the probability estimated by using Monte Carlo simulation. The matched results demonstrate the correct derivation of the closed form with propagated channel uncertainties. In particular, the transmit power of the sink is shown as a function of the OP in each of the three environment settings (sub-urban, urban, and dense-urban) in Fig. 3. First, it is obvious that the OP curves of the investigated system are lower in a sub-urban environment than those in urban or dense-urban areas. This is due to the fact that higher obstructions occur in urban and dense-urban settings, leading to the likelihood of the LoS being greater than that of the NLoS. Second, when the sink transmit power rises, the OP of the sensors falls. This is because an increase in the sink's transmit power results in a corresponding increase in power at the UAVR.

In Fig. 4, we plot the OP as a function of the number of antennas and the altitude of the UAVR. According to the graph, increasing h_R

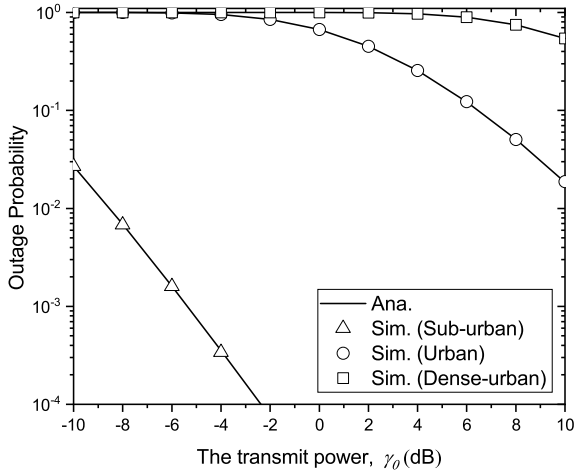

Fig. 3. The OP versus the transmit power of the sink with three environments: sub-urban, urban, and dense-urban.

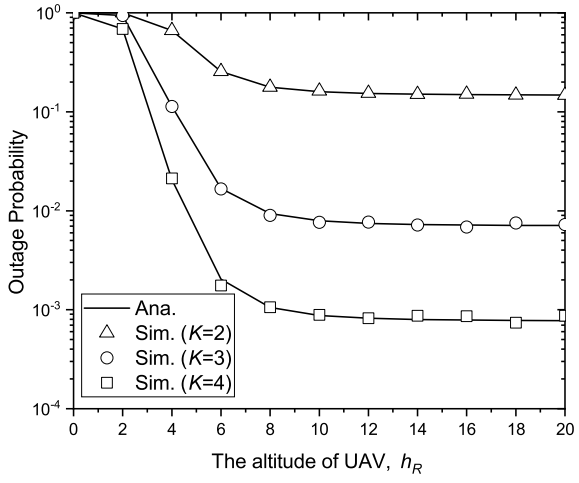

Fig. 4. The OP versus the altitude of the UAVR with $K = 2$, $K = 3$, and $K = 4$.

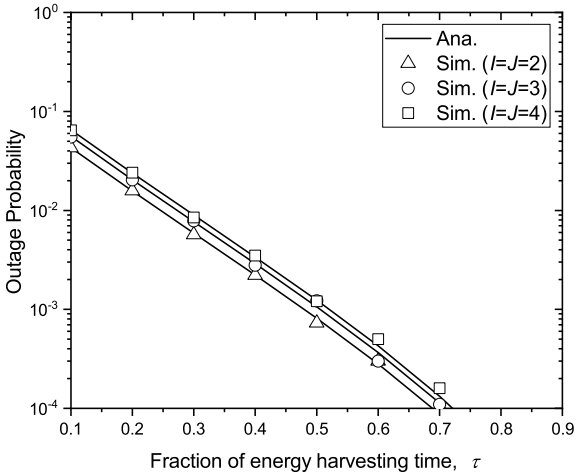

Fig. 5. The OP versus the fraction of EH with $I = J = 2$, $I = J = 3$, and $I = J = 4$.

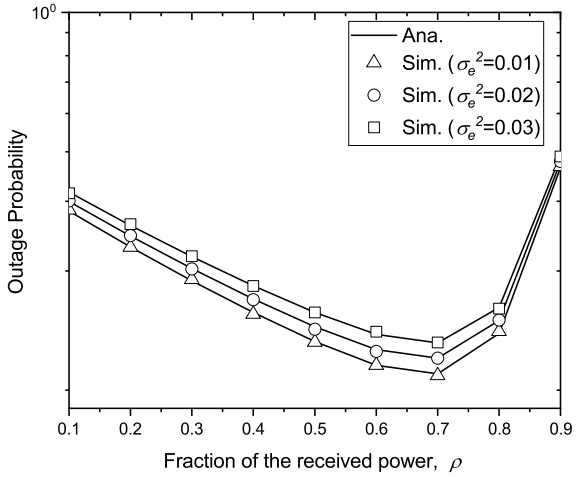

Fig. 6. The OP versus the fraction of receiver power at the UAVR with $\sigma_e^2 = 0.01$, $\sigma_e^2 = 0.02$, and $\sigma_e^2 = 0.03$.

reduces $\mathcal{P}$ and once h_R reaches an intermediate point $h_R = 18$, $\mathcal{P}$ is convergence. This is because the probability of LoS conditions are more likely to occur when the UAVR flies at a high altitude. As a result, the overall efficiency of the system improves. However, at really high altitudes, path loss also increases significantly. Thus, the SINR at the sensors is solely dependent on the direct link from the sink to the sensors. It can be observed from Fig. 4 that the OP decreases by $2 \times 10^{-1}, 10^{-2}$ and 10^{-3} as the number of antennas on the UAVR increases by $K = 2, K = 3$, and $K = 4$, respectively. The rationale behind this phenomenon lies in the fact that the diversity gain exhibits a positive correlation with the overall quantity of antennas. However, if K is too large, the hardware complexity and the computing power to choose the best antenna for the UAVR will increase. Therefore, in practical deployment, the number of antennas K should be indicated first, at the highest value, so that the hardware can be deployed. Then, optimization will be conducted later for other optimal parameters, including the UAVR's 3D position.

In the following paragraphs, we show the impact of the fraction of EH time at the UAVR on the OP with the different numbers of the sensors in Fig. 5. As shown in this figure, when the EH time increases, the OP decreases. This is due to the fact that higher τ results in higher transmit power at the UAVR. Furthermore, increasing the number of sensors leads to a decrease in the OP. Because the worst sensors (i.e., U_{i*} and V_{j*}) are picked depending on the channel conditions, increasing the number of sensors increases the range of choices for the worst sensors.

Fig. 6 illustrates the effect of the fraction of receiver power at the UAVR with the difference of the channel estimation errors $\sigma_{e_{XY}}^2 = 0.01$, $\sigma_{e_{XY}}^2 = 0.02$, and $\sigma_{e_{XY}}^2 = 0.03$ on the OP. We can see from this Fig. that the OP decreases first as the ρ increases, and then the ρ reaches a certain point where the OP increases. This is due to the fact that the higher ρ leads to the larger harvested energy at the UAVR. However, when ρ is much larger, the power for information transmission from the sink to UAVR decreases, resulting in poor signal strength at the UAVR. This leads to a rise in the OP of sensors. Furthermore, the results also show that the OP of the system improves as $\sigma_{e_{XY}}^2$ decreases. This is because as the uncertainty in the channel estimate grows, so does our ignorance about the channel.

Next, we present the optimization results using BAO as stated in Algorithm 1. We formulate the bat λ_i as the candidate solution with six parameters: ρ, α_u, β_u, and the UAV position in 3D space x, y, and z. Specifically, the search space contains all the candidate vectors with the form described as (49). In such, the bounds for α_u and β_u are $[0.5, 1]$. The generation limit G is set to 40 and the bat population N_λ to 20. The loudness A_i and the pulse rate r_i are sampled from the uniform distribution $U(0, 1)$ while the constant for loudness update $\alpha = 0.5$ and

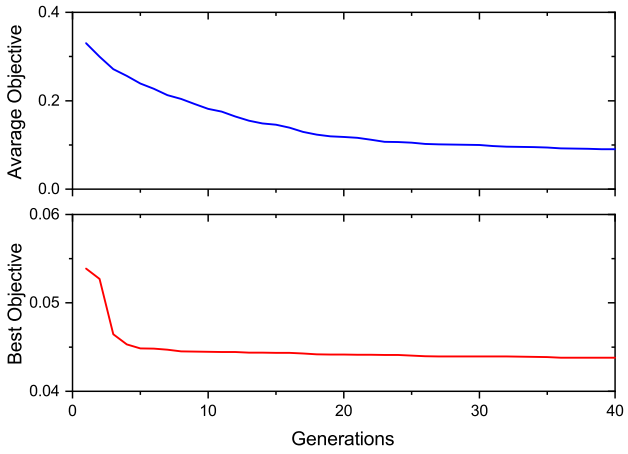

Fig. 7. Convergence characteristics on the current Best objective value and the Average objective value over generations.

the constant for pulse rate update $\gamma = 0.5$. The objective function $F(\lambda)$ is defined as $\mathcal{P}$ in (45).

Fig. 7 illustrates the changes of the bat population objective values over generations. Note that the objective values are not called fitness in this work because we are trying to minimize these values while fitness is a metric usually for maximizing. In stead, objective values can be referred to as "weakness values". Besides, the curves in Fig. 7 are the results from averaging 20 random times of running BAO in order to highlight the trends of the curves, not the fluctuations. The upper curve is for the average objective value of the whole bat population, which reduces gradually from 0.3301 to 0.0902. This indicates that the optimization process or the BAO works well and obtains convergence.

Likewise, the lower curve tracks the objective value of the current best candidate over generations, or iterations of evolving. This curve achieves lower and lower value and gets stable value of 0.0438 at generation 38, 39, and 40. It is remarkable that the average objective value decreases gradually but the best objective value does sharply at the beginning generations. This means the BAO is good at exploring the search space and quickly sends bats to different local areas around minima. After the better local minima are explored, many bats are allowed to move towards the good bats at a lower and lower probability due to (49) and (54), making exploitation be more and more focused. As the result, the best objective value decreases gradually in the next generations. Obviously, BAO is good at both exploration and exploitation and should be recommended for similar multi-variate non-convex optimization problems in continuous search space.

6. Conclusions

In this paper, we focused on the OP minimization problem for a hybrid TS/PS SWIPT-enabled cooperative NOMA IoT network by using the UAVR. In particular, the communication process is divided into three phases: the EH and direct information transmission phase, the information decoding phase, and the relaying transmission phase. Herein, the energy-limited UAVR is powered by the sink node based on the hybrid TS/PS SWIPT scheme. We have obtained a mathematical expression that gives a closed-form solution for the OP at the sensors so that we can test how well the system works. Then, we used a BAO algorithm to determine the optimal fraction of received power, power allocation coefficients, and the position of the UAVR so that the OP at the sensors is as low as possible. The analytical results verified by the Monte-Carlo simulations have indicated that the system performance is improved by increasing either the number of antennas or the altitude of the UAVR. Finally, these results have shown that BAO is good at both exploration and exploitation for the multi-variate non-convex optimization problems in the similar considered network. In our future work, we will generate the training data based on heuristic search methods and then apply a deep learning model to learn the relationship between conditional parameters and the optimal parameters. This helps to later predict the optimal parameters of the enhanced cooperative NOMA IoT architecture. This future work can enable rapid adaptation to environmental conditions in general systems with their large-scale network sizes, mobility, and interference mitigations [44,45].

CRediT authorship contribution statement

Van Nhan Vo: Conceptualization, Formal analysis, Investigation, Methodology, Validation, Visualization, Writing – original draft, Writing – review & editing. **Viet-Hung Dang:** Conceptualization, Software, Validation, Visualization, Writing – original draft. **Hung Tran:** Resources, Software, Validation, Visualization, Writing – original draft. **Duc-Dung Tran:** Investigation, Methodology, Resources, Visualization, Writing – original draft. **Symeon Chatzinotas:** Validation, Visualization, Writing – review & editing. **Hai Le Quoc:** Resources, Software, Validation, Visualization, Writing – original draft. **Chakchai So-In:** Conceptualization, Data curation, Supervision, Writing – review & editing. **Van-Truong Truong:** Validation, Visualization, Writing – original draft. **Tu Dac Ho:** Conceptualization, Funding acquisition, Methodology, Supervision, Validation, Writing – review & editing.

Declaration of competing interest

1. We have none of conflict in interest for submitting this paper.
2. The main author and the co-authors have none of conflict in interest.
3. Also, the corresponding author is a professor from Norwegian University of Since and Technology, who has a publishing agreement with Alexandria Engineering Journal. So, the publishing fee will be included in this agreement once the paper is accepted.

Acknowledgment

This work was supported by grants from the Norwegian University of Science and Technology (NTNU) and Duy Tan University.

References

[1] W.C. Ng, et al., Resource optimization for UAV-assisted wireless power charging enabled hybrid coded edge computing network, IEEE Trans. Mob. Comput. (2023) 1–17, http://dx.doi.org/10.1109/TMC.2023.3246994.
[2] M. Shi, K. Yang, D. Niyato, H. Yuan, H. Zhou, Z. Xu, The meta distribution of SINR in UAV-assisted cellular networks, IEEE Trans. Commun. 71 (2) (2023) 1193–1206, http://dx.doi.org/10.1109/TCOMM.2022.3233064.
[3] G. Sun, J. Li, A. Wang, Q. Wu, Z. Sun, Y. Liu, Secure and energy-efficient UAV relay communications exploiting collaborative beamforming, IEEE Trans. Commun. 70 (8) (2022) 5401–5416, http://dx.doi.org/10.1109/TCOMM.2022.3184160.
[4] J. Tang, G. Chen, J.P. Coon, Secrecy performance analysis of wireless communications in the presence of UAV jammer and randomly located UAV eavesdroppers, IEEE Trans. Inf. Forensics Secur. 14 (11) (2019) 3026–3041.
[5] X. Sun, D.W.K. Ng, Z. Ding, Y. Xu, Z. Zhong, Physical layer security in UAV systems: Challenges and opportunities, IEEE Wireless Commun. 26 (5) (2019) 40–47.
[6] N.H. Motlagh, T. Taleb, O. Arouk, Low-altitude unmanned aerial vehicles-based internet of things services: Comprehensive survey and future perspectives, IEEE Internet of Things J. 3 (6) (2016) 899–922.
[7] B. Ji, Y. Li, B. Zhou, C. Li, K. Song, H. Wen, Performance analysis of UAV relay assisted IoT communication network enhanced with energy harvesting, IEEE Access 7 (2019) 38738–38747.
[8] X. Liu, S. Wang, C. Yin, Biological intelligence inspired trajectory design for energy harvesting UAV networks, Sensors 23 (2) (2023) 1–18.
[9] Y. Gu, S. Aissa, RF-based energy harvesting in decode-and-forward relaying systems: Ergodic and outage capacities, IEEE Trans. Wireless Commun. 14 (11) (2015) 6425–6434.
[10] A. Nasir, X. Zhou, S. Durrani, R. Kennedy, Wireless-powered relays in cooperative communications: Time-switching relaying protocols and throughput analysis, IEEE Trans. Commun. 63 (5) (2015) 1607–1622.

[11] P. Liu, S. Gazor, I.-M. Kim, D.I. Kim, Noncoherent relaying in energy harvesting communication systems, IEEE Trans. Wireless Commun. 14 (12) (2015) 6940–6954.

[12] S. Atapattu, J. Evans, Optimal energy harvesting protocols for wireless relay networks, IEEE Trans. Wireless Commun. 15 (8) (2016) 5789–5803, http://dx.doi.org/10.1109/TWC.2016.2569097.

[13] Z. Chen, Z. Ding, X. Dai, R. Zhang, A mathematical proof of the superiority of NOMA compared to conventional OMA, IEEE Trans. Signal Process. (2016) 1–28.

[14] Z. Ding, F. Adachi, H.V. Poor, The application of MIMO to non-orthogonal multiple access, IEEE Trans. Wireless Commun. 15 (1) (2016) 537–552.

[15] C. Guo, L. Zhao, C. Feng, Z. Ding, H.-H. Chen, Energy harvesting enabled NOMA systems with full-duplex relaying, IEEE Trans. Veh. Technol. 68 (7) (2019) 7179–7183.

[16] A.A. Nasir, H.D. Tuan, T.Q. Duong, H.V. Poor, UAV-enabled communication using NOMA, IEEE Trans. Commun. 67 (7) (2019) 5126–5138, http://dx.doi.org/10.1109/TCOMM.2019.2906622.

[17] D.-D. Tran, S.K. Sharma, S. Chatzinotas, I. Woungang, B. Ottersten, Short-packet communications for MIMO NOMA systems over Nakagami-m fading: BLER and minimum blocklength analysis, IEEE Trans. Veh. Technol. 70 (4) (2021) 3583–3598, http://dx.doi.org/10.1109/TVT.2021.3066367.

[18] N. Ashraf, S.A. Sheikh, S.A. Khan, I. Shayea, M. Jalal, Simultaneous wireless information and power transfer with cooperative relaying for next-generation wireless networks: A review, IEEE Access 9 (2021) 71482–71504, http://dx.doi.org/10.1109/ACCESS.2021.3078703.

[19] T.M. Hoang, L.T. Dung, B.C. Nguyen, X.H. Le, X.N. Tran, T. Kim, Outage Probability and Throughput of Mobile Multiantenna UAV-Assisted FD-NOMA Relay System With Imperfect CSI, IEEE Systems J. 17 (1) (2023) 1477–1488, http://dx.doi.org/10.1109/JSYST.2022.3180797.

[20] F. Khennoufa, K. Abdellatif, F. Kara, H. Kaya, X. Li, K. Rabie, et al., A hybrid energy harvesting protocol for cooperative NOMA: Error performance approach, 2022, arXiv:2207.00133.

[21] H.M.A. Abdullah, A.V.S. Kumar, HFSA-SORA: Hybrid firefly simulated annealing based spectrum opportunistic routing algorithm for cognitive radio Ad hoc networks (CRAHN), in: Proc. Intern. Conf. Intelligent Comput. and Control, 2017, pp. 1–10.

[22] F. Okoli, J. Bert, S. Abdelaziz, N. Boussion, D. Visvikis, Optimizing the beam selection for noncoplanar VMAT by using simulated annealing approach, IEEE Trans. Radiat. Plasma Med. Sci. 6 (5) (2022) 609–618.

[23] D.K. Luong, M. Ali, Y.F. Hu, J.P. Li, R. Asif, K. Abdo, Simulated annealing-based multilink selection algorithm in SDN-enabled avionic networks, IEEE Access 9 (2021) 145301–145316.

[24] A.M. Yesaswini, K. Annapurna, GA and PSO based spectrum allotment in cognitive radio networks, in: Intern. Conf. Inventive Computat. Techn., 2021, pp. 701–704.

[25] H.E.S. Hassan, A.E.D.S. Hafez, A.A. Saied, Optimum cognitive radio networks performance in AWGN using genetic algorithm, in: Intern. Telecommun. Conf., 2021, pp. 1–4.

[26] M.G.C. P., V. T., Analysis and performance evaluation of PSO for spectrum allocation in CRN, in: Intern. Conf. Innovative Practices Techno. and Management, 2021, pp. 119–124.

[27] M. Yan, H. Yuan, J. Xu, Task allocation and route planning of multiple UAVs in a marine environment based on an improved particle swarm optimization algorithm, EURASIP J. Adv. Signal Process. 2021 (94) (2021) 1–23.

[28] Z. Liu, J. Liu, F. Zhou, R.W. Liu, N. Xiong, A robust GA/PSO-Hybrid algorithm in intelligent shipping route planning systems for maritime traffic networks, J. Internet Technol. 19 (6) (2019) 1635–1644.

[29] Y. Luo, C. Wu, Y. Leng, N. Huang, L. Mao, J. Tang, Throughput Optimization for NOMA Cognitive Relay Network with RF Energy Harvesting Based on Improved Bat Algorithm, Mathematics 10 (22) (2022) http://dx.doi.org/10.3390/math10224357.

[30] Y. Li, R. Zhang, J. Zhang, S. Gao, L. Yang, Cooperative jamming for secure UAV communications with partial eavesdropper information, IEEE Access 7 (2019) 94593–94603.

[31] Y. Chen, N. Zhao, Z.D.M.-S. Alouini, Multiple UAVs as relays: Multi-hop single link versus multiple dual-hop links, IEEE Trans. Wireless Commun. 17 (9) (2018) 6348–6359.

[32] M.F. Sohail, C.Y. Leow, S. Won, Non-orthogonal multiple access for unmanned aerial vehicle assisted communication, IEEE Access 6 (2018) 22716–22727.

[33] A. Abbasi, A. Seifi, A novel method mixed power flow in transmission and distribution systems by using master-slave splitting method, Electr. Power Compon. Syst. 36 (11) (2008) 1141–1149.

[34] A. Abbasi, A. Seifi, Fast and perfect damping circuit for ferroresonance phenomena in coupling capacitor voltage transformers, Electr. Power Compon. Syst. 37 (4) (2009) 393–402.

[35] A. Abbasi, S. Abbasi, J. Ansari, E. Rahmani, Effect of plug-in electric vehicles demand on the renewable micro-grids, J. Intell. Fuzzy Systems 29 (5) (2015) 1957–1966.

[36] M. Vosoogh, M. Kamyar, A. Akbari, A. A. Abbasi, A novel modification approach based on MTLBO algorithm for optimal management of renewable micro-grids in power systems, J. Intell. Fuzzy Systems 27 (1) (2014) 465–473.

[37] B. Ji, Y. Li, S. Chen, C. Han, C. Li, H. Wen, Secrecy outage analysis of UAV assisted relay and antenna selection for cognitive network under nakagami-m channel, IEEE Trans. Cogn. Commun. Netw. 7 (2020) 1–11, http://dx.doi.org/10.1109/TCCN.2020.2965945.

[38] T.-L. Nguyen, D.-T. Do, Power allocation schemes for wireless powered NOMA systems with imperfect CSI: An application in multiple antenna-based relay, Int. J. Commun. syst. 31 (15) (2018) 1–17.

[39] Y. Ye, R.Q. Hu, G.L.L. Shi, Enhance latency-constrained computation in MEC networks using uplink NOMA, IEEE Trans. Commun. 68 (4) (2020) 2409–2425.

[40] V.N. Vo, T.G. Nguyen, C. So-In, H. Tran, Outage performance analysis of energy harvesting wireless sensor networks for NOMA transmissions, Mobile Netw. Appl. 25 (2020) 23–41.

[41] H. Tran, T.X. Quach, H. Tran, E. Uhlemann, Optimal energy harvesting time and transmit power in cognitive radio network under joint constraints of primary users and eavesdroppers, in: Proc. Int. Symp. on Personal, Indoor and Mobile Radio Commun., 2017, pp. 1–8.

[42] D.-T. Do, M. Vaezi, T.-L. Nguyen, Wireless powered cooperative relaying using NOMA with imperfect CSI, in: Proc. IEEE Globecom, Abu Dhabi, U.A.E, 2018, pp. 1–6.

[43] A.M. Hayaneh, S.A.R. Zaidi, D.C. Mclernon, M.D. Renzo, M. Ghogho, Performance analysis of UAV enabled disaster recovery networks: A stochastic geometric framework based on cluster processes, IEEE Access 6 (2018) 26215–26230.

[44] H. Chiroma, A.S. Noor, S. Abdulkareem, A.I. Abubakar, A. Hermawan, H. Qin, M.F. Hamza, T. Herawan, Neural networks optimization through genetic algorithm searches: A review, Appl. Math. Inf. Sci. 11 (2017) 1543–1564.

[45] M.H. Behiry, M. Aly, Cyberattack detection in wireless sensor networks using a hybrid feature reduction technique with AI and machine learning methods, J. of Big Data 16 (2024) (2024) 1–39.